THE JOURNAL OF PHYSICAL CHEMISTRY B
A JOURNAL OF THE AMERICAN CHEMICAL SOCIETY

pubs.acs.org/JPCB

Article

Long-Range Interface Effects in Room Temperature Ionic Liquids: Vibrational Lifetime Studies of Thin Films

John P. Breen, Laura C. Leibfried, Xiangyu Xing, and Michael D. Fayer*

Cite This: https://doi.org/10.1021/acs.jpcb.3c02948

Read Online

ACCESS | Metrics & More | Article Recommendations | Supporting Information

ABSTRACT: Interface effects in the room temperature ionic liquids (RTILs) 1-butyl-3-methylimidazolium tetrafluoroborate ($BmimBF_4$) and 1-butyl-3-methylimidazolium bis(trifluoromethylsulfonyl)imide ($BmimNTf_2$) were investigated using ultrafast infrared polarization selective pump−probe (PSPP) spectroscopy. The CN stretch mode of SCN^- dissolved in the RTILs was used as the vibrational probe. The vibrational lifetime of the SCN^- was the experimental observable. Quite similar single SCN^- lifetimes were observed: 59.5 ± 0.4 ps in bulk $BmimBF_4$ and 56.4 ± 0.4 ps in bulk $BmimNTf_2$. Thin films of both RTILs with thicknesses in the range of 15−300 nm were prepared by spin coating on functionalized substrates. PSPP experiments were performed in a small-incidence reflection geometry. In the thin films, a second, shorter lifetime was observed in addition to the bulk lifetime, with the amplitude of the shorter lifetime increasing with decreasing film thickness. By modeling the thickness dependence of the lifetime amplitudes, the correlation length of the interface effect (constant for exponential falloff of the influence of the interface) was determined to be 44.6 ± 0.6 nm for $BmimBF_4$ and 48.3 ± 2.2 nm for $BmimNTf_2$. The values for the shorter film lifetimes were 12.6 ± 0.1 ps for $BmimBF_4$ and 20.2 ± 0.6 ps for $BmimNTf_2$; the substantial differences from the bulk lifetimes showed that some of the SCN^- anions near the interface experience an environment distinct from that of the bulk. It was also found that for the $BmimNTf_2$ sample only, some of the SCN^- anions reside in the surface functionalized layer with two distinct environments having distinct lifetimes.

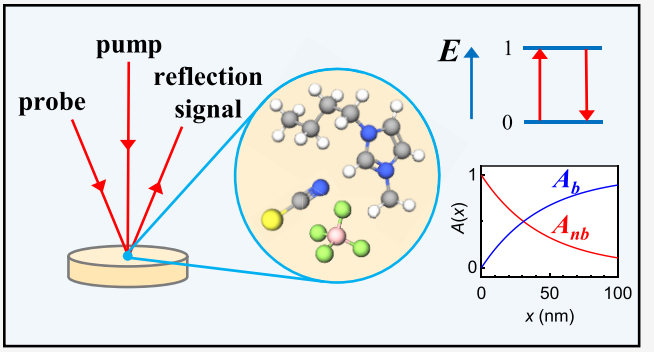

1. INTRODUCTION

Room temperature ionic liquids (RTILs) are salts that are liquids at ambient temperatures. They often consist of bulky and asymmetric ions with delocalized charges.[1,2] RTILs have many applications as electrolytes in batteries[3,4] and capacitors,[5,6] media in CO_2 capture,[7,8] solvents in chemical synthesis,[9,10] lubricants,[11,12] and propellants.[13,14] The properties of RTILs near interfaces are relevant to many of these applications. The interfacial behavior of RTILs has been studied using a variety of techniques, including surface force apparatus,[15−18] atomic force microscopy,[18−20] X-ray reflectivity,[21,22] neutron reflectometry,[23,24] sum frequency generation spectroscopy,[25,26] confocal fluorescence microscopy,[27] and molecular dynamics simulations.[28,29] Some studies have shown that the effect of a solid interface can propagate for tens or hundreds of nanometers in RTILs.[17,18,27,30] The dynamics of RTILs in poly(ether sulfone) membranes were studied by ultrafast infrared spectroscopy[31] and time-dependent Stokes shift measurements,[32] which showed that the dynamics of confined RTILs can be significantly slower than those in the bulk, even in pores with diameters of ∼300 nm.

A method for preparing thin films of the RTIL 1-butyl-3-methylimidazolium bis(trifluoromethylsulfonyl)imide ($BmimNTf_2$) with controllable thickness in the range of 15−300 nm was reported previously.[33] The $BmimNTf_2$ dynamics as a function of film thickness were studied with two-dimensional infrared (2D IR) spectroscopy in the near-Brewster reflection geometry.[34] The results showed that the dynamics are extraordinarily slow at the interface, and the effect of the interface propagates into the liquid for tens of nanometers.[33] An additional 2D IR study of films as a function of the cation chain length revealed that longer chains result in the interface effect falling off more quickly with distance from the surface.[35] The dependence of the dynamics on the substrate functionalized layer thickness was also investigated by 2D IR. The functionalized surface layer contains bound cations. Increased layer thickness (1−2 nm) containing more bound cations results in slower spectral diffusion (slower structural fluctuations) of the RTIL comprising the thin films.[36]

Received: May 4, 2023
Revised: June 10, 2023

In this paper, we extend these previous studies by applying another ultrafast infrared technique, polarization selective pump−probe (PSPP) spectroscopy, to RTIL thin films. These experiments used SCN^-, introduced into the RTIL as BmimSCN, as the vibrational probe. A small-incidence reflection geometry was used to avoid theoretical complications that arise when performing the PSPP experiment in the near-Brewster reflection geometry.[37] Two quantities can be extracted from the PSPP experiment; the first is the population decay of the vibrationally excited state (i.e., the vibrational lifetime), and the second is the orientational correlation function, which describes the reorientation of the molecules. In this work, we discuss only the lifetime results; the orientational relaxation will be described in a forthcoming publication, in which experimental and theoretical considerations necessary to obtain useful data are presented. In addition, this study investigated the effect of different RTIL anions by performing PSPP experiments on the tetrafluoroborate RTIL $BmimBF_4$ as well as on $BmimNTf_2$.

Changes in vibrational lifetimes upon confinement have been observed previously in chemical systems including water in reverse micelles,[38,39] Nafion fuel cell membranes,[40] and clay minerals;[41] 1-methylimidazole in mesoporous silica;[42] and metal carbonyls in Pd_6L_4 nanocages.[43] Because the vibrational lifetime is sensitive to the local chemical and structural environment,[44] the thickness dependence of the lifetime data gives information about the length scale of the interface effect as well as the differences between the interfacial and bulk structures. Therefore, the vibrational lifetime data are complementary to the previously measured 2D IR data. One advantage of the lifetime as an observable is that the population decay can be measured with a high signal-to-noise ratio over the entire relevant time range. In contrast, in 2D IR experiments with slow dynamics, it may not be possible to measure the entire decay, which adds additional uncertainty to the results for the thinnest films that display the slowest dynamics.[33]

2. EXPERIMENTAL METHODS

Triethoxy-3-(2-imidazolin-1-yl)propylsilane (97%) and 1-iodobutane (99%) were purchased from Sigma-Aldrich. Toluene (99.5%), ethanol (200 proof, 99.5%), and methanol (extra dry, 99.8%) were obtained from Fisher Chemical. The RTILs 1-butyl-3-methylimidazolium tetrafluoroborate ($BmimBF_4$, 99%), 1-butyl-3-methylimidazolium bis-(trifluoromethylsulfonyl)imide ($BmimNTf_2$, 99.5%), and 1-butyl-3-methylimidazolium thiocyanate (BmimSCN, 98%) were purchased from Iolitec. $BmimBF_4$, BmimSCN, and $BmimNTf_2$ were dried under vacuum at 80 °C for 7, 5, and 3 days, respectively. After drying, the RTILs were transferred into a nitrogen-filled glovebox with a typical trace moisture content of 0.5 ppm, where all subsequent handling took place. The water contents of the dried $BmimBF_4$, $BmimNTf_2$, and BmimSCN were measured with Karl Fischer titration to be 56, 18, and 14 ppm, respectively. These low concentrations of trace water have a negligible effect on RTIL dynamics.[45]

2.1. Substrate Functionalization. The substrates for the samples in this study must satisfy two requirements: (1) they must transmit the infrared wavelengths used in the experiments, and (2) the top layer of the substrate must be of a type such that the RTIL will wet it effectively, spreading out to form a film instead of droplets. Therefore, CaF_2 windows with a 100 nm layer of SiO_2 deposited on the upper surface were purchased from New Wave Optics, and then the SiO_2 surface was chemically functionalized with a positively charged network of molecules which mimic the structure of the $Bmim^+$ cation, as described previously.[33] This functionalization step was necessary because RTIL thin films cannot be made directly on CaF_2 or SiO_2 surfaces.[33]

The functionalization procedure, which has been described in detail in previous publications,[33,36] is a two-step reaction. In the first step, neutral imidazoline molecules are attached to the surface using the terminal OH groups of the SiO_2. In the second step, the imidazoline molecules are converted to imidazolinium cations by a reaction with 1-iodobutane. The total number of imidazolinium cations bound to the substrate surface is proportional to the duration of the first step of the reaction. The surface layer thickness can be controlled by adjusting the length of time that the first step of the reaction is allowed to run.[36] In the present study, the step 1 reaction was run for 12 h for all of the substrates.

In the second step of the surface functionalization reaction, a butyl group from the 1-iodobutane is attached to imidazolinium, and I^- is formed. Prior to the spin coating of the RTIL on the functionalized surface, iodides are the counterions for the imidazolium cations. When BF_4^- is the RTIL anion, it is small enough to enter the surface layer. It displaces the iodides because of the vastly larger number of BF_4^-'s compared to the number of I^-'s or SCN^- probe molecules. When the films are washed off the surface layer, the iodides that are in the RTIL film are removed. Spin coating the same thickness film on the washed surface layer functionalized substrate produces a film that gives identical experimental results to those from the first sample. Therefore, the small amount of I^- in the initial RTIL film does not change the film's properties. When NTf_2^- is the anion, it is too large to fit into the surface layer matrix. As discussed in detail below, because the RTIL anions cannot replace the iodides in the surface layer, the SCN^- probe does so because they also far outnumber the I^-'s. In all cases, the imidazolium cations will be charge compensated by anions, either iodides when the surface layer is initially formed or anions from the RTIL that is spin coated onto the surface functionalized substrate.

2.2. Sample Preparation. The RTIL thin films were prepared by spin coating, as described in previous publications.[33,35,36] All of the sample preparation was performed in a nitrogen-filled glovebox. First, the vibrational probe BmimSCN was added to $BmimBF_4$ and to the $BmimNTf_2$. This choice of vibrational probe avoids introducing small cations (e.g., K^+), which are known to perturb the dynamics of RTILs.[46] In addition, the SCN^- anion has a relatively large transition dipole and a reasonably long vibrational lifetime,[47−49] which are important for achieving sufficient signal-to-noise ratios in the PSPP experiments. $BmimBF_4$ and BmimSCN were mixed in a 50:1 molar ratio, and $BmimNTf_2$ and BmimSCN were mixed in a 20:1 molar ratio. These ratios were determined by performing PSPP experiments on the bulk RTILs as a function of the vibrational probe concentration to find the highest vibrational probe concentration that does not perturb the dynamics (Figure S1).

Next, a spin-coating precursor solution was prepared by dissolving a small portion of the 50:1 $BmimBF_4$:BmimSCN or 20:1 $BmimNTf_2$:BmimSCN mixture in methanol. The ratio of RTIL to methanol was chosen based on the desired thickness of the film. For $BmimBF_4$:BmimSCN, the ratios of mg of RTIL per g of methanol were 100, 38.5, 13.2, and 4.20 for film

https://doi.org/10.1021/acs.jpcb.3c02948
J. Phys. Chem. B XXXX, XXX, XXX−XXX

thicknesses of 301, 127, 49, and 15 nm, respectively. For $BmimNTf_2$:BmimSCN, the ratios of mg of RTIL per g of methanol were 128, 47.3, 16.0, and 5.15 for film thicknesses of 312, 128, 48, and 14 nm, respectively. The solutions were passed through 0.22 μm syringe filters, and then 150 μL of the solution was loaded onto a functionalized substrate. The substrate was spun for 30 s at 3000 rpm to form the RTIL film. The RTIL film/substrate was then assembled into a sealed cell by stacking an O-ring and another CaF_2 window on top of the RTIL film and tightening the cell with a threaded retention ring. This sealed cell allowed the RTIL film to continue to be shielded from atmospheric moisture after removal from the glovebox.

Methanol, unlike water, evaporates readily from the spin-coated films. To test for residual methanol in the films, we added methanol to the bulk RTILs, and we took FT-IR spectra. A new peak was observed at 3574 cm^{-1}. FT-IR spectra are taken of all thin film samples. We can observe peaks that are a fraction of an mOD. Even in the thickest films, we do not observe the 3574 cm^{-1} peak. Therefore, there is very little or no residual methanol in the RTIL films.

"Post film" samples were prepared by making an RTIL film, as discussed above, then removing the film by sonicating the substrate in ethanol for 10 min, and then drying the substrate using a flow of nitrogen gas. This resulted in a sample with no film but with a remaining functionalized surface layer, which could be investigated using the linear and nonlinear infrared experiments.

2.3. Linear Infrared Spectra. Each sample's linear absorbance spectrum was measured using a Thermo-Fisher Nicolet 6700 FT-IR instrument. These measurements were made in transmission with an incident angle of 15°. Because of the weak absorbance of the RTIL thin films, the linear spectra required substantial averaging to obtain reasonable signal-to-noise, especially for the thinner films. The number of scans acquired ranged from 256 for the thickest films to 2048 scans for the thinnest films.

The thickness of each thin film sample was determined from the linear spectrum using the absorbance in the aromatic C−H region. For $BmimBF_4$, there are three peaks at 3107, 3126, and 3163 cm^{-1}; for $BmimNTf_2$, the three peaks are located at 3105, 3125, and 3160 cm^{-1} (Figure S2). The three overlapping peaks were fit simultaneously with three Gaussian functions, and the resulting area of the highest frequency peak was compared with that of bulk samples with known thickness. The highest frequency peak was used because it has the largest separation from the other peaks, and it is the peak with the largest absorption; therefore, it will give the most accurate results. The linear spectrum of the functionalized substrate with no film was subtracted before the fitting procedure.

For analysis of the SCN^- region of the FT-IR spectra, an additional subtraction was performed in which the spectrum of a pure $BmimBF_4$ or a pure $BmimNTf_2$ sample was scale-subtracted. The scaling factor was adjusted to minimize the remaining aliphatic C−H peaks (2800−3000 cm^{-1}) in the subtraction result.

2.4. Infrared Polarization Selective Pump−Probe Spectroscopy. The ultrafast infrared laser system used for these experiments has been described in detail in previous publications.[33,34] A Ti:sapphire oscillator/regenerative amplifier system produces pulses with a center wavelength of 800 nm, a pulse energy of 2 mJ, and a repetition rate of 3 kHz. The 800 nm pulses pump a home-built optical parametric amplifier (OPA), which generates two colors of near-infrared light at wavelengths of ∼1.4 and 1.9 μm, which are then used to generate mid-infrared (MIR) via difference frequency generation (DFG). For the experiments in this work, the OPA and DFG setup was adjusted such that the MIR spectrum was centered at 2054 cm^{-1}, which is the peak of the SCN^- absorbance for the RTIL samples studied (Figure 1). The pulse energy and pulse duration of the MIR were ∼25 μJ and ∼180 fs.

The MIR is split into a strong (90%) pump beam and a weak (10%) probe beam. The pump beam passes through a germanium acousto-optic modulator (AOM) pulse shaping system,[50,51] which for the pump−probe experiments operates on a four-shot cycle where the first and third shots are "on" but with opposite phase, and the second and fourth shots are "off". This allows for collection of the pump−probe signal and removal of scattered light from the sample.[51] The probe beam travels down a mechanical delay line, which is scanned during the experiment to acquire data with various pump−probe delays.

As the pump−probe delay is increased, the pump−probe signal amplitude will change for two reasons: (1) population relaxation from the vibrationally excited state to the ground state and (2) reorientation of the probe molecules. To separate these two effects, a polarization selective pump−probe (PSPP) experiment is used, which measures two polarizations, parallel and perpendicular, with respect to the incident pump polarization.[52,53] Then the parallel and perpendicular signals are given by

$$S_{\parallel}(t) = P(t)(1 + 0.8C_2(t)) \quad (1)$$

$$S_{\perp}(t) = P(t)(1 - 0.4C_2(t)) \quad (2)$$

where $P(t)$ is the population decay and $C_2(t)$ is the second Legendre polynomial orientational correlation function. In this study, we are only interested in $P(t)$, which is given by

$$P(t) = \frac{1}{3}(S_{\parallel}(t) + 2S_{\perp}(t)) \quad (3)$$

In the pump−probe experiment, a single pump pulse interacts twice with the sample, and a probe pulse interacts once, inducing a third-order polarization in the sample, which emits a nonlinear signal collinear with the probe pulse. The probe pulse serves as the local oscillator (LO), and the experimental observable is the heterodyne signal, i.e., the modulation of the LO field by the signal field. The combined signal and LO are sent to a monochromator configured as a spectrograph, which disperses the beams onto a mercury cadmium telluride (MCT) array detector with 32 pixels, allowing for simultaneous detection of the pump−probe signal at 32 separate frequencies over a total range of ∼40 cm^{-1}.

For thin samples like the RTIL films in this study, it is desirable to perform the experiments in reflection, which can significantly enhance the heterodyne signal.[34] This phenomenon results from the fact that in reflection the LO (the reflected probe pulse) is attenuated, but the signal field is essentially unaffected, increasing the amplitude of the heterodyne signal. The largest enhancement comes from using a p-polarized probe beam and setting the incident angle of the probe beam close to Brewster's angle, and this near-Brewster reflection geometry has been successfully implemented for various 2D IR experiments.[33−37] However, for PSPP experiments, it is not straightforward to perform the

https://doi.org/10.1021/acs.jpcb.3c02948
J. Phys. Chem. B XXXX, XXX, XXX−XXX

experiment with such large incident angles because then the out-of-plane projections of the pump and probe beams onto the sample introduce significant theoretical complications.[37] Briefly, the observed "parallel" and "perpendicular" signals will be mixtures of the pure parallel and perpendicular signals, and therefore eq 3 will not give the correct $P(t)$. In addition, for the orientational relaxation, which can also be measured with PSPP experiments, the usual formula (eq S1 in the Supporting Information) will not give the correct results.

Consequently, the experiments in this study were performed in a small-incidence reflection geometry, where the incident angles were kept small (probe incident angle = 18°, pump incident angle = 2°) to minimize the out-of-plane projections of the beams onto the sample.[37] Calculations show that for these angles the distortion of the $P(t)$ measurement is negligible.[37] The polarization of the probe beam was +90° (vertical, corresponding to s-polarized light, which eliminates the out-of-plane projection of the probe beam); the polarization of the pump beam was +45°, and then the reflection signal and LO passed through a resolving polarizer set at ±45° to acquire the parallel and perpendicular signals. The resolved signal and LO then passed through an additional polarizer at 0° so that the beam entering the monochromator always has the same polarization, regardless of the angle of the resolving polarizer.[53] The near normal reflection geometry produces a signal enhancement of ∼5 compared to that of a transmission experiment. In a subsequent publication experimental methods and theory will be presented for obtaining accurate $P(t)$ data and orientational relaxation data in the near-Brewster geometry, which can increase the signal >30 over a transmission experiment.

For samples with thicknesses that are a significant fraction of the MIR wavelength, there is an additional complication of performing the experiment in reflection. The signals emitted by molecules at different depths in the sample are phase-shifted relative to each other. Consequently, a dispersive component is introduced into the signal.[34] This causes the pump−probe signal to shift in frequency, altering the apparent frequency dependence of the data (Figure S3). Therefore, the experiments on the relatively thick ∼300 nm films were performed in transmission to avoid the dispersive feature; in transmission, the signals from different depths in the sample are in phase, regardless of the total sample thickness.[34] Experiments on all thinner films, for which the dispersive component was negligible, were performed in reflection.

The pump pulses produced by the laser in this study are relatively strong. At the sample, the maximum pulse energy is ∼6 μJ and the spot size is ∼160 μm. Therefore, it is important to ensure that the pump energy is not so high that it causes undesired effects, such as saturation of the vibrational transition or higher-order interactions. The dependence on the pump power of the bulk RTIL PSPP results was measured by using the AOM pulse shaping system to decrease the amount of light diffracted. The results at early time differ when low pump power vs high pump power is used, likely due to a transition saturation effect. Therefore, the pump beam was attenuated until the results became independent of any additional lowering of the pump power, and all experiments were performed with this reduced pump power (∼1.5 μJ).

3. RESULTS AND DISCUSSION

3.1. Infrared Linear Spectra. For both $BmimBF_4$ and $BmimNTf_2$, the SCN^- peak in the bulk RTIL is asymmetric with a wing on the red side of the band (Figure 1). This can be clearly seen by fitting the blue half of the peak with a Voigt line shape and then extending the fit curve to lower frequency. As seen in Figure 1, the fit underestimates the experimental data on the red side of the peak. Similar asymmetric thiocyanate spectra have been observed in other chemical systems and have been attributed to the non-Condon effect, i.e., a frequency-dependent transition dipole, which is larger on the red side of the line.[54,55] The asymmetry observed in this study is believed to arise from this same phenomenon; further evidence for this is provided in Section 3.2.

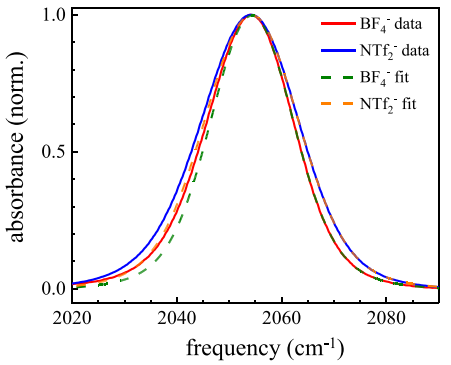

Figure 1. Normalized FT-IR spectra of SCN^- anions in bulk $BmimBF_4$ (solid red curve) and $BmimNTf_2$ (solid blue curve). The center positions of the peaks are the same, but in $BmimNTf_2$ the peak is somewhat wider. Voigt fits (dashed curves) to the high-frequency halves of the peaks and extended to lower frequency are narrower than the experimental spectra on the low-frequency side, indicating that the peaks are asymmetric. This asymmetry arises from the non-Condon effect (the transition dipole increases at lower frequency).

A comparison of the SCN^- peaks in the two bulk RTILs shows that they have essentially identical center frequencies, but in $BmimNTf_2$ the peak is somewhat wider. Voigt fits of the entire peaks give center frequencies of 2053.91 ± 0.01 and 2053.87 ± 0.01 cm^{-1} and full width at half-maximum (FWHM) values of 20.0 ± 0.1 and 22.5 ± 0.1 cm^{-1} for $BmimBF_4$ and $BmimNTf_2$, respectively. The vibrational frequency of the SCN^- anion depends on its interaction with the surrounding liquid. Hydrogen bonding will affect the vibrational frequency, with stronger interactions resulting in higher frequencies.[56] In imidazolium RTILs, the SCN^- anion mainly interacts with the cation; hydrogen bonding between the SCN^- nitrogen and the C2 hydrogen of the imidazolium ring plays a major role.[57] SCN^- can also make very weak H-bonds with C4 and C5.[58] The changed RTIL anion affects the extent of RTIL anion−cation hydrogen bonding.[59,60] This in turn may change the distribution of interactions between SCN^- and the cation, leading to different widths of the SCN^- peak in $BmimBF_4$ and $BmimNTf_2$.

Figure 2 shows the FT-IR spectra of SCN^- in the thin films. The absorbance in these samples ranges from a few mOD to <1 mOD, resulting in noisy spectra. In thin films of both $BmimBF_4$ and $BmimNTf_2$, the SCN^- peak appears to become wider with decreasing thickness, while the center frequencies are not significantly affected (Figure 2a,b). This suggests that the SCN^- anions close to the interface experience a broader distribution of environments than those in the bulk liquid. However, quantitative analysis of the thin film spectra is hindered by poor signal-to-noise in the spectra of the thinnest films.

https://doi.org/10.1021/acs.jpcb.3c02948
J. Phys. Chem. B XXXX, XXX, XXX−XXX

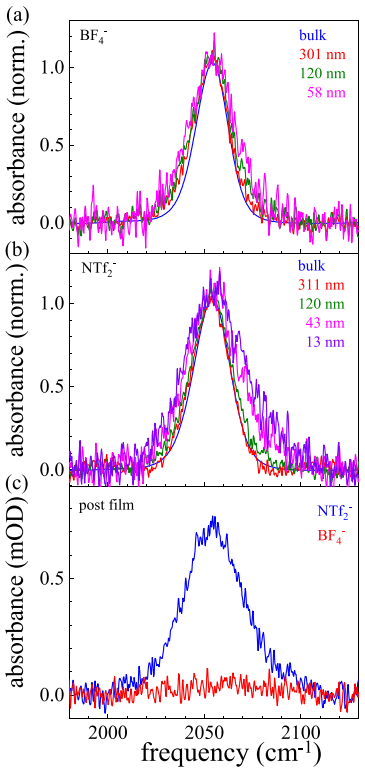

Figure 2. FT-IR spectra of SCN^- anions in RTIL samples of various thicknesses. (a) Normalized spectra for $BmimBF_4$ films as well as the bulk liquid. (b) Normalized spectra for $BmimNTf_2$ films as well as the bulk liquid. In the thin film samples, the SCN^- peak becomes wider with decreasing thickness. (c) Spectra for the functionalized surface layer only (post film samples) made by removing $BmimBF_4$ and $BmimNTf_2$ films via sonication. In the post film samples, for $BmimNTf_2$ a significant amount of SCN^- absorbance is observed, indicating the presence of residual SCN^- anions in the substrate surface layer. In the $BmimBF_4$ surface layer there is negligible SCN^- absorbance.

In post film samples prepared from $BmimNTf_2$ films, a significant SCN^- peak was observed (Figure 2c). This suggests that when a $BmimNTf_2$ film is prepared, a large number of SCN^- anions go into the functionalized surface layer of the substrate and that they remain there when the $BmimNTf_2$ film is removed. The successful removal of the $BmimNTf_2$ film was confirmed by the disappearance of the C−H and S−O absorbance bands from the $Bmim^+$ and NTf_2^- ions in the FT-IR spectra (Figure S4). By comparing the SCN^- absorbance of $BmimNTf_2$ films, which is the sum of the absorbance from the film and the absorbance from the surface layer, to the absorbance of the post film samples, the number of SCN^- in the surface layer was estimated to be the equivalent of the number of SCN^- in a ∼43 nm film. The true thickness of the surface layer is likely to be only ∼2 nm, based on ellipsometry measurements reported for a similar system.[61] Therefore, the large amount of SCN^- absorbance from the surface layer suggests that the SCN^- concentration is much higher in the surface layer than in the thin film. A possible explanation for this relates to the large size of the NTf_2^- anion.[62,63] The bulky NTf_2^- anions likely do not fit into the surface layer network, and therefore the only anions able to enter the network are the SCN^- anions.

When post film samples were made from $BmimBF_4$ films, negligible SCN^- absorbance was observed (Figure 2c). This suggests that the concentration of the SCN^- anions in the surface layer is quite low in this case. This result demonstrates that the BF_4^- can fit into the surface layer network due to its small size,[62,63] which dilutes the concentration of SCN^-. Because of the low concentration of SCN^- in the solution, it is virtually eliminated from the surface layer.

3.2. Infrared Lifetime Data. *3.2.1. Bulk Lifetimes.* In bulk $BmimBF_4$ and bulk $BmimNTf_2$, the population decay near the center of the SCN^- peak is a single exponential (Figure 3, green curves with fits). The lifetime values from the single-exponential fits are 59.5 ± 0.4 and 56.4 ± 0.4 ps for $BmimBF_4$ and $BmimNTf_2$, respectively. The vibrational lifetime depends on the coupling of the CN stretch mode to intra- and intermolecular modes because vibrational relaxation occurs by creating and annihilating other modes, as required to conserve energy.[44] Given the large differences in the structures of the anion, the small difference between the SCN^- lifetimes in $BmimBF_4$ and $BmimNTf_2$ indicates that the RTIL anions play only a minor role in the relaxation of vibrationally excited SCN^- anions. In the relaxation process, most of the excited CN stretch energy is transferred to intramolecular modes.[37] As the intramolecular modes, S−CN stretch and two degenerate bends, do not exactly match the CN stretch energy, energy is conserved by creating or annihilating one or more modes of

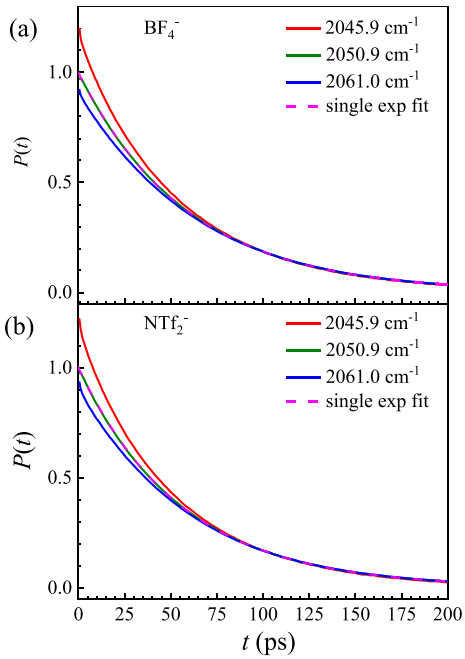

Figure 3. Normalized pump−probe population decays for bulk RTILs (a) $BmimBF_4$ and (b) $BmimNTf_2$. Decays are shown for three frequencies: one on the low-frequency side of the peak (2045.9 cm^{-1}), one near the peak center (2050.9 cm^{-1}), and one on the high-frequency side (2061.0 cm^{-1}). The decays have been normalized such that their values match at t = 100 ps. In both RTILs, a single-exponential fit (dashed magenta line) to the decay at 2050.9 cm^{-1} after t = 100 ps, and then extended to t = 0 ps, fits the center frequency (2050.9 cm^{-1}) decay well, even at early time, but overestimates the 2061.0 cm^{-1} decay and underestimates the 2045.9 cm^{-1} decay at early time. The data and fit indicate the presence of a rise on the high-frequency side, and an additional decay on the low-frequency side, which is consistent with population flowing from low frequency to high frequency, which arises from uneven pumping due to the non-Condon effect.

https://doi.org/10.1021/acs.jpcb.3c02948
J. Phys. Chem. B XXXX, XXX, XXX−XXX

the liquid continuum. The relaxation will depend on the coupling and the density of states of the continuum at the frequency required to conserve energy. Because of the large difference in the two anions, it is unlikely that the coupling and density of states will be the same. The fact that the two lifetimes are so similar suggests that coupling of CN to intermolecular degrees of freedom may principally involve the cation.

Away from the SCN^- peak center, the population decay is not a single exponential. For both $BmimBF_4$ and $BmimNTf_2$, a single-exponential fit to long time ($t > 100$ ps) misses the early time data; the fit overestimates the data for high frequencies and underestimates the data for low frequencies (Figure 3). Therefore, there is a rise at early time in the high-frequency data and an additional decay at early time in the low-frequency data. This type of behavior has been observed previously.[54,64] It is caused by spectral diffusion in which there is a net flow of population from the low-frequency side of the band to the high-frequency side. The population flow can occur if the initial excited state population distribution is not an equilibrium distribution. This phenomenon is attributed to the non-Condon effect, in which the frequency-dependent transition dipole of the SCN^- anion leads to uneven pumping of the band, generating a nonequilibrium excited-state population distribution.[54,64] These observations of the non-Condon effect in population decay are consistent with the asymmetric FT-IR spectra discussed in Section 3.1.

3.2.2. $BmimBF_4$ Thin Film Lifetimes. In a film of $BmimBF_4$ with a thickness of 127 nm, the population decay at the center frequency does not fit to a single exponential. Instead, a biexponential fit is required, and the two time constants are ~13 and 59 ps. This multiexponential behavior will not arise from a non-Condon effect because the magnitude of the non-Condon effect is generally small near the center frequency as observed for the bulk samples.[64,65] Instead, the biexponential lifetime decay suggests that there are two ensembles of SCN^- anions that have distinct vibrational lifetimes. As discussed above, the vibrational lifetime is sensitive to the local environment because the rate of vibrational relaxation depends on which modes are present in the surrounding solvent and the coupling to those modes.[44] Therefore, the observation of two lifetimes indicates that there are two distinct environments in the $BmimBF_4$ films. The longer film lifetime is the same as the bulk lifetime, while the shorter film lifetime is substantially shorter than the bulk, suggesting that in the film some of the SCN^- anions experience a bulklike environment, while other anions are in a very different environment.

As the $BmimBF_4$ film thickness decreases, the overall population decay becomes faster (Figure 4a). Each thickness can be fit with a biexponential with time constants of 13 and 59 ps, but the amplitudes of the two components vary with film thickness. This thickness dependence demonstrates that the same two environments are present in the films, but their relative probabilities change with distance from the interface. As the film becomes thinner, the relative amplitude of the short lifetime increases. Therefore, the probability of finding the nonbulk environment increases with proximity to the interface. A possible explanation for this is that the interfacial structure of the RTIL stabilizes a nonbulk configuration, lowering its energy relative to that of the bulk configuration, so that the nonbulk configuration dominates near the interface. As the interfacial effect falls off with increasing distance from the surface, the stabilizing effect on the nonbulk configuration decreases, making it increasingly unfavorable for the nonbulk configuration to occur. The result is that the amplitude of the nonbulk component decreases as the film thickness increases.

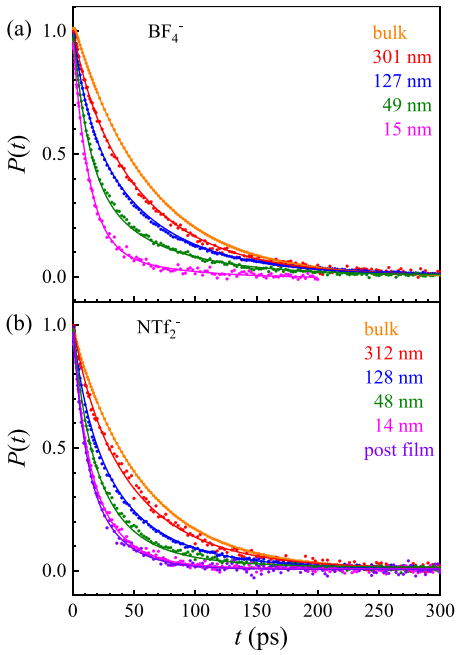

Figure 4. Normalized pump−probe population decays (points) at 2053.4 cm^{-1} for the bulk liquids, thin film samples, and post film samples, along with fits (solid curves) from the models described in the text, for (a) $BmimBF_4$ samples and (b) $BmimNTf_2$ samples.

This observation that the lifetime amplitudes, but not the lifetimes themselves, depend on the film thickness suggests a model consisting of a depth-dependent population decay with amplitudes $A_{nb}(x)$ and $A_b(x)$ that depend on x, the distance from the functionalized solid interface:

$$P_{film}(t, x) = A_{nb}(x) \exp(-t/\tau_{nb}) + A_b(x) \exp(-t/\tau_b) + y_0 \quad (4)$$

τ_{nb} (nonbulk) is the shorter lifetime, τ_b is the longer lifetime (bulk), and y_0 is an offset (which may be nonzero due to a heating signal in the pump−probe experiment). For a discussion of an alternative model with a depth-dependent lifetime, which results in a lower quality fit to the data, see the Supporting Information. Statistical analysis discussed in the Supporting Information shows that the depth-dependent lifetime model is not plausible.

In order to match the experimental trend, as x increases, $A_{nb}(x)$ must decrease, and $A_b(x)$ must increase. In addition, for large values of x, the population decay should converge to bulk behavior, which implies that $A_{nb}(x) \to 0$ as $x \to \infty$. We adopt exponential functional forms for $A_{nb}(x)$ and $A_b(x)$ because these satisfy the criteria described above and result in a good fit to the experimental data. Other functional forms with more abrupt spatial changes, such as step functions, for $A_{nb}(x)$ and $A_b(x)$ could not fit the data well. For data that have been normalized to a maximum amplitude of one, the formulas for the amplitudes are

$$A_{nb}(x) = \exp(-x/L) \quad (5)$$

$$A_b(x) = 1 - \exp(-x/L) \quad (6)$$

https://doi.org/10.1021/acs.jpcb.3c02948
J. Phys. Chem. B XXXX, XXX, XXX−XXX

where L is the correlation length which describes the distance over which the interface effect falls off. A plot of the amplitude functions is shown in Figure S5. This model is similar to the modified two-state model previously used to describe the spatial dependence of orientational relaxation in water and 1-methylimidazole confined in mesoporous silica.[42,66]

The experimentally observed population decay is the average over all of the SCN^- anions throughout all depths of the film:

$$P_{avg}(t) = \frac{1}{d_{film}} \int_0^{d_{film}} P_{film}(t, x)\, dx \tag{7}$$

where d_{film} is the film thickness.

Equation 7 was used to simultaneously fit the population decay data for the four thicknesses of $BmimBF_4$ films at the center frequency. The analysis was restricted to the center frequency to avoid possible contributions to the population decay from the non-Condon effect (see the Supporting Information). τ_{nb} and L were shared among the thicknesses, and τ_b was fixed to the bulk lifetime of 59.5 ps. As shown in Figure 4a, the model fit all four thicknesses very well. The model fit gave output values of τ_{nb} = 12.6 ± 0.1 ps and L = 44.6 ± 0.6 nm.

The thin film samples have two interfaces: One is the functionalized substrate, which contains bound cations with presumably compensating BF_4^- anions, which will result in large dipoles. The other is a neutral interface consisting of nitrogen gas. The model used here assumes that only the functionalized solid interface has an effect on the lifetime of the nearby ions. An alternative approach is to assume that the two interfaces have identical effects, which would lead to a decrease in the correlation length by a factor of 2. The decision not to include an effect for the neutral interface is based on previous experiments which showed that if the surface is functionalized with neutral species, there is a much smaller effect on the RTIL thin film correlation length associated with spectral diffusion measured with 2D IR than when the solid surface is functionalized with bound cations.[36] In addition, recent simulations of RTIL/vacuum interfaces show that the effect of such an interface has decayed within a few nanometers of the interface.[67]

The correlation length of 44.6 nm reported here for $BmimBF_4$ thin films is comparable to the value found in our previous study of $BmimNTf_2$ thin films using 2D IR spectroscopy.[35] The previous study used a model that assumed two identical interfaces and determined the correlation length to be 21.6 nm; if the effect of the neutral interface had been neglected, then the correlation length would have been 43.2 nm. The assumption that the N_2 interface had a large influence was based on early simulations, which indicated that the RTIL/vacuum interface had a large long-range influence on the RTIL structure.[68] As mentioned above, recent simulations show that the effect of an RTIL/vacuum interface propagates into the RTIL for only a few nanometers.[67]

The present results are consistent with previous ultrafast infrared results showing long-range interface effects in RTIL thin films; in the previous 2D IR studies, spectral diffusion (structural dynamics) slowed dramatically as the film becomes thinner.[33,35,36] For thin films, the time scale of the spectral diffusion was much slower than the vibrational lifetime, which made determination of the correlation length less certain. Here, we look at the population decay, for which the time scale of the decay is the vibrational lifetime, and therefore the entire decay can be measured within the experimentally accessible time window, which simplifies the analysis. The current study provides additional evidence that the propagation distance of RTIL interface effects is very long compared to the <2 nm interface effect length scales observed in conventional liquids such as water,[38,39,66] benzene,[69,70] and acetonitrile.[71]

3.2.3. $BmimNTf_2$ Thin Film Lifetimes. The analysis of the lifetime data for the $BmimNTf_2$ thin film samples is complicated by a significant contribution to the pump–probe signal from SCN^- anions in the substrate functionalized surface layer. As discussed in Section 3.1, FT-IR spectra of post film samples prepared from $BmimNTf_2$ films showed that such samples have SCN^- absorbances corresponding to the equivalent of the absorbance of ~43 nm of film. Therefore, we assume that this amount of surface layer signal is present in the $BmimNTf_2$ film data.

PSPP experiments were performed on these post film samples (purple data in Figure 4b), and the population relaxation at the center frequency was found to decay as a biexponential:

$$P_{surface}(t) = A_{1,surface} \exp(-t/\tau_{1,surface}) + (1 - A_{1,surface}) \times \exp(-t/\tau_{2,surface}) + y_{0,surface} \tag{8}$$

The time constants were $\tau_{1,surface}$ = 8.4 ± 1.0 ps and $\tau_{2,surface}$ = 27 ± 4 ps with the relative amplitude $A_{1,surface}$ = 0.48 ± 0.09. The presence of two lifetimes indicates that the SCN^- anions in the surface layer are in two distinct environments, and both environments are different from those experienced in the bulk RTILs because both surface layer lifetimes are substantially shorter than the bulk lifetimes.

We assume that the population decay in the $BmimNTf_2$ thin films has the same functional form as that in the $BmimBF_4$ thin films. Therefore, eqs 4–6 apply to the film portion of the $BmimNTf_2$ data. Then, to incorporate the surface layer signal, eq 7 was modified to become

$$P_{avg}(t) = \frac{1}{d_{film} + d_{surface}} \left(P_{surface}(t) d_{surface} + \int_0^{d_{film}} P_{film}(t, x)\, dx \right) \tag{9}$$

Assuming that the behavior of the SCN^- anions in the surface layer, as well as their signal amplitude, was unaffected by the presence of a $BmimNTf_2$ thin film, $d_{surface}$ was set to 43 nm and $P_{surface}(t)$ was given by eq 8. $d_{surface}$ is an empirical value used to produce the proper weighting in the data of the surface and film contributions.

The four thicknesses of $BmimNTf_2$ thin films were fit simultaneously with eq 9. τ_{nb} and L were shared among the thicknesses, and τ_b was fixed to the bulk $BmimNTf_2$ lifetime of 56.4 ps. The model fit all four thicknesses quite well (Figure 4b), and the output values were τ_{nb} = 20.2 ± 0.6 ps and L = 48.3 ± 2.2 nm.

The $BmimNTf_2$ correlation length is very similar to that for $BmimBF_4$ (Section 3.2.2). Therefore, for these two liquids, the identity of the anion does not have a large effect on the propagation distance of the interface effect. Also, the $BmimNTf_2$ correlation length determined in the present study from the lifetime data is comparable to the $BmimNTf_2$ value previously measured using 2D IR spectroscopy,[35] which is 43.2 nm after accounting for a difference in the models (see Section 3.2.2). One difference between the $BmimNTf_2$ data and the $BmimBF_4$ data is the value of the shorter lifetime τ_{nb}

https://doi.org/10.1021/acs.jpcb.3c02948
J. Phys. Chem. B XXXX, XXX, XXX−XXX

(20.2 ps in $BmimNTf_2$, 12.6 ps in $BmimBF_4$); this suggests that the environment around the short-lifetime SCN^- anions is different in the two RTILs. However, caution should be used when interpreting the $BmimNTf_2$ results due to the additional uncertainties associated with the procedure of accounting for the surface layer signal.

4. CONCLUDING REMARKS

We have studied the vibrational lifetimes of SCN^- anions in $BmimBF_4$ and $BmimNTf_2$, both in bulk liquids and in thin films, using infrared polarization selective pump−probe spectroscopy. In each bulk liquid, the population decay near the center frequency was a single exponential, indicating that there is a single environment surrounding the ensemble of SCN^- anions. A more complicated behavior away from the line center was attributed to the non-Condon effect.[54,55,64,65] The SCN^- lifetimes in bulk $BmimBF_4$ and $BmimNTf_2$ were 59.5 ± 0.4 and 56.4 ± 0.4 ps, respectively. The small difference between these two values indicates that the RTIL anions do not play a large role in the vibrational relaxation of the SCN^- anions.

In thin films of $BmimBF_4$, two lifetimes were observed. One lifetime was bulklike, while the other was about 5 times shorter. Experiments on thin films with thicknesses in the range of 15−300 nm revealed that the relative amplitude of the faster lifetime increased as the films became thinner. This observation of two lifetimes implied the existence of two distinct environments within the films, and the varying amplitude indicated that the relative probability of finding the short-lifetime environment decreased with the distance from the interface. The amplitude decrease with distance was modeled as an exponential decay. Fitting the data yielded a correlation length (exponential decay constant) of L = 44.6 ± 0.6 nm. The short lifetime value was determined to be τ_{nb} = 12.6 ± 0.1 ps.

In $BmimNTf_2$ thin films, additional considerations were necessary to account for the effect of a significant number of SCN^- anions on the functionalized surface layer. The functionalized surface makes it possible to form high quality thin films with controlled thicknesses by spin coating. The surface layer contains covalently bound cations, propylbutylimidazolinium, and the SCN^- entered the layer for charge compensation, which indicates that the NTf_2^- anions are too large to enter the 1−2 nm surface layer network created by functionalization. When the anion was BF_4^-, no SCN^- was observed in the surface layer because the much smaller BF_4^- anion could enter the surface network, virtually eliminating the presence of SCN^-.

For the $BmimNTf_2$ samples, population decay of the surface layer signal was measured by performing a polarization selective pump−probe experiment on samples created by removing $BmimNTf_2$ films by sonication. A biexponential decay was observed for the surface layer population decay, showing that there are two well-defined environments for the SCN^-. The population decay contribution from the surface layer was included in modeling the $BmimNTf_2$ film data. The model fitting resulted in a correlation length of L = 48.3 ± 2.2 nm and a short lifetime of τ_{nb} = 20.2 ± 0.6 ps. The similar correlation lengths for the $BmimBF_4$ and $BmimNTf_2$ indicate that the choice of BF_4^- vs NTf_2^- does not significantly affect the length scale of the interface effect on the thin film structure.

The correlation lengths are similar to the value previously determined for $BmimNTf_2$ using another ultrafast infrared technique, 2D IR spectroscopy,[35] and are substantially longer than those observed for conventional liquids like water,[38,39,66] benzene,[69,70] and acetonitrile.[71] These results agree with previous studies in showing that interface effects in RTILs can propagate over long distances. A previous 2D IR study, which reports on structural fluctuation in the thin films, shows that the nature of the surface functionalization can have a large impact on the effect of the surface.[36] The long-range influence of an interface has implications for RTIL applications in which behavior at interfaces is important, such as at battery electrodes[3,4] or in membranes for CO_2 capture.[7,8] Even tens of nanometers away from the interface, RTIL behavior can be significantly different from that of the bulk liquid. Therefore, bulk properties may not be good guides for the behavior of RTILs in the vicinity of interfaces.

■ ASSOCIATED CONTENT

Supporting Information

The Supporting Information is available free of charge at https://pubs.acs.org/doi/10.1021/acs.jpcb.3c02948.

Figures S1−S9 (PDF)

■ AUTHOR INFORMATION

Corresponding Author

Michael D. Fayer − *Department of Chemistry, Stanford University, Stanford, California 94305, United States;* orcid.org/0000-0002-0021-1815; Phone: 650 723-4446; Email: fayer@stanford.edu

Authors

John P. Breen − *Department of Chemistry, Stanford University, Stanford, California 94305, United States*

Laura C. Leibfried − *Department of Chemistry, Stanford University, Stanford, California 94305, United States*

Xiangyu Xing − *Department of Chemistry, Stanford University, Stanford, California 94305, United States*

Complete contact information is available at: https://pubs.acs.org/10.1021/acs.jpcb.3c02948

Notes

The authors declare no competing financial interest.

■ ACKNOWLEDGMENTS

This work was supported by the Air Force Office of Scientific Research Grant FA9550-16-1-0104.

■ REFERENCES

(1) Castner Jr, E. W.; Margulis, C. J.; Maroncelli, M.; Wishart, J. F. Ionic Liquids: Structure and Photochemical Reactions. *Annu. Rev. Phys. Chem.* **2011**, *62*, 85−105.

(2) Hayes, R.; Warr, G. G.; Atkin, R. Structure and Nanostructure in Ionic Liquids. *Chem. Rev.* **2015**, *115*, 6357−6426.

(3) Matsumoto, H.; Sakaebe, H.; Tatsumi, K. Preparation of Room Temperature Ionic Liquids Based on Aliphatic Onium Cations and Asymmetric Amide Anions and Their Electrochemical Properties as a Lithium Battery Electrolyte. *J. Power Sources* **2005**, *146*, 45−50.

(4) Park, J.-W.; Yamauchi, K.; Takashima, E.; Tachikawa, N.; Ueno, K.; Dokko, K.; Watanabe, M. Solvent Effect of Room Temperature Ionic Liquids on Electrochemical Reactions in Lithium-Sulfur Batteries. *J. Phys. Chem. C* **2013**, *117*, 4431−4440.

(5) Frackowiak, E.; Lota, G.; Pernak, J. Room-Temperature Phosphonium Ionic Liquids for Supercapacitor Application. *Appl. Phys. Lett.* **2005**, *86*, 164104.
(6) Galiński, M.; Lewandowski, A.; Stępniak, I. Ionic Liquids as Electrolytes. *Electrochim. Acta* **2006**, *51*, 5567−5580.
(7) Bara, J. E.; Camper, D. E.; Gin, D. L.; Noble, R. D. Room-Temperature Ionic Liquids and Composite Materials: Platform Technologies for CO_2 Capture. *Acc. Chem. Res.* **2010**, *43*, 152−159.
(8) Hasib-ur-Rahman, M.; Siaj, M.; Larachi, F. Ionic Liquids for CO_2 Capture—Development and Progress. *Chem. Eng. Proc.* **2010**, *49*, 313−322.
(9) Hallett, J. P.; Welton, T. Room-Temperature Ionic Liquids: Solvents for Synthesis and Catalysis. 2. *Chem. Rev.* **2011**, *111*, 3508−3576.
(10) Haumann, M.; Riisager, A. Hydroformylation in Room Temperature Ionic Liquids (RTILs): Catalyst and Process Developments. *Chem. Rev.* **2008**, *108*, 1474−1497.
(11) Liu, W.; Ye, C.; Gong, Q.; Wang, H.; Wang, P. Tribological Performance of Room-Temperature Ionic Liquids as Lubricant. *Trib. Lett.* **2002**, *13*, 81−85.
(12) Ye, C.; Liu, W.; Chen, Y.; Yu, L. Room-Temperature Ionic Liquids: A Novel Versatile Lubricant. *Chem. Commun.* **2001**, 2244−2245.
(13) Shamshina, J. L.; Smiglak, M.; Drab, D. M.; Parker, T. G.; Dykes, H. W. H., Jr.; Di Salvo, R.; Reich, A. J.; Rogers, R. D. Catalytic Ignition of Ionic Liquids for Propellant Applications. *Chem. Commun.* **2010**, *46*, 8965−8967.
(14) Zhang, Q.; Shreeve, J. M. Energetic Ionic Liquids as Explosives and Propellant Fuels: A New Journey of Ionic Liquid Chemistry. *Chem. Rev.* **2014**, *114*, 10527−10574.
(15) Gebbie, M. A.; Valtiner, M.; Banquy, X.; Fox, E. T.; Henderson, W. A.; Israelachvili, J. N. Ionic Liquids Behave as Dilute Electrolyte Solutions. *Proc. Nat. Acad. Sci. U. S. A.* **2013**, *110*, 9674−9679.
(16) Perkin, S. Ionic Liquids in Confined Geometries. *Phys. Chem. Chem. Phys.* **2012**, *14*, 5052−5062.
(17) Bou-Malham, I.; Bureau, L. Nanoconfined Ionic Liquids: Effect of Surface Charges on Flow and Molecular Layering. *Soft Matter* **2010**, *6*, 4062−4065.
(18) Jurado, L. A.; Kim, H.; Arcifa, A.; Rossi, A.; Leal, C.; Spencer, N. D.; Espinosa-Marzal, R. M. Irreversible Structural Change of a Dry Ionic Liquid under Nanoconfinement. *Phys. Chem. Chem. Phys.* **2015**, *17*, 13613−13624.
(19) Atkin, R.; Warr, G. G. Structure in Confined Room-Temperature Ionic Liquids. *J. Phys. Chem. C* **2007**, *111*, 5162−5168.
(20) Hayes, R.; El Abedin, S. Z.; Atkin, R. Pronounced Structure in Confined Aprotic Room-Temperature Ionic Liquids. *J. Phys. Chem. B* **2009**, *113*, 7049−7052.
(21) Carmichael, A. J.; Hardacre, C.; Holbrey, J. D.; Nieuwenhuyzen, M.; Seddon, K. R. Molecular Layering and Local Order in Thin Films of 1-Alkyl-3-Methylimidazolium Ionic Liquids Using X-Ray Reflectivity. *Mol. Phys.* **2001**, *99*, 795−800.
(22) Sloutskin, E.; Ocko, B. M.; Tamam, L.; Kuzmenko, I.; Gog, T.; Deutsch, M. Surface Layering in Ionic Liquids: An X-Ray Reflectivity Study. *J. Am. Chem. Soc.* **2005**, *127*, 7796−7804.
(23) Benedetto, A.; Heinrich, F.; Gonzalez, M. A.; Fragneto, G.; Watkins, E.; Ballone, P. Structure and Stability of Phospholipid Bilayers Hydrated by a Room-Temperature Ionic Liquid/Water Solution: A Neutron Reflectometry Study. *J. Phys. Chem. B* **2014**, *118*, 12192−12206.
(24) Bowers, J.; Vergara-Gutierrez, M. C.; Webster, J. R. Surface Ordering of Amphiphilic Ionic Liquids. *Langmuir* **2004**, *20*, 309−312.
(25) Iimori, T.; Iwahashi, T.; Kanai, K.; Seki, K.; Sung, J.; Kim, D.; Hamaguchi, H.-o.; Ouchi, Y. Local Structure at the Air/Liquid Interface of Room-Temperature Ionic Liquids Probed by Infrared-Visible Sum Frequency Generation Vibrational Spectroscopy: 1-Alkyl-3-Methylimidazolium Tetrafluoroborates. *J. Phys. Chem. B* **2007**, *111*, 4860−4866.
(26) Rivera-Rubero, S.; Baldelli, S. Surface Spectroscopy of Room-Temperature Ionic Liquids on a Platinum Electrode: A Sum Frequency Generation Study. *J. Phys. Chem. B* **2004**, *108*, 15133−15140.
(27) Ma, K.; Jarosova, R.; Swain, G. M.; Blanchard, G. J. Charge-Induced Long-Range Order in a Room-Temperature Ionic Liquid. *Langmuir* **2016**, *32*, 9507−9512.
(28) Lynden-Bell, R.; Kohanoff, J.; Del Popolo, M. Simulation of Interfaces between Room Temperature Ionic Liquids and Other Liquids. *Faraday Discuss.* **2005**, *129*, 57−67.
(29) Yan, T.; Li, S.; Jiang, W.; Gao, X.; Xiang, B.; Voth, G. A. Structure of the Liquid-Vacuum Interface of Room-Temperature Ionic Liquids: A Molecular Dynamics Study. *J. Phys. Chem. B* **2006**, *110*, 1800−1806.
(30) Anaredy, R. S.; Shaw, S. K. Long-Range Ordering of Ionic Liquid Fluid Films. *Langmuir* **2016**, *32*, 5147−5154.
(31) Shin, J. Y.; Yamada, S. A.; Fayer, M. D. Dynamics of a Room Temperature Ionic Liquid in Supported Ionic Liquid Membranes Vs the Bulk Liquid: 2D IR and Polarized IR Pump-Probe Experiments. *J. Am. Chem. Soc.* **2017**, *139*, 311−323.
(32) Thomaz, J. E.; Bailey, H. E.; Fayer, M. D. The Influence of Mesoscopic Confinement on the Dynamics of Imidazolium-Based Room Temperature Ionic Liquids in Polyether Sulfone Membranes. *J. Chem. Phys.* **2017**, *147*, 194502.
(33) Nishida, J.; Breen, J. P.; Wu, B.; Fayer, M. D. Extraordinary Slowing of Structural Dynamics in Thin Films of a Room Temperature Ionic Liquid. *ACS Cent. Sci.* **2018**, *4*, 1065−1073.
(34) Nishida, J.; Yan, C.; Fayer, M. D. Enhanced Nonlinear Spectroscopy for Monolayers and Thin Films in near-Brewster's Angle Reflection Pump-Probe Geometry. *J. Chem. Phys.* **2017**, *146*, 094201.
(35) Wu, B.; Breen, J. P.; Fayer, M. D. Structural Dynamics in Ionic Liquid Thin Films: The Effect of Cation Chain Length. *J. Phys. Chem. C* **2020**, *124*, 4179−4189.
(36) Wu, B.; Breen, J. P.; Xing, X.; Fayer, M. D. Controlling the Dynamics of Ionic Liquid Thin Films Via Multilayer Surface Functionalization. *J. Am. Chem. Soc.* **2020**, *142*, 9482−9492.
(37) Xing, X.; Li, J.; Breen, J. P.; Nishida, J.; Karunadasa, H. I.; Fayer, M. D. Probing Lattice Dynamics in Two-Dimensional Inorganic Pseudohalide Perovskites with Ultrafast Infrared Spectroscopy. *J. Phys. Chem. C* **2022**, *126*, 10145−10158.
(38) Fenn, E. E.; Wong, D. B.; Giammanco, C. H.; Fayer, M. Dynamics of Water at the Interface in Reverse Micelles: Measurements of Spectral Diffusion with Two-Dimensional Infrared Vibrational Echoes. *J. Phys. Chem. B* **2011**, *115*, 11658−11670.
(39) Moilanen, D. E.; Fenn, E. E.; Wong, D.; Fayer, M. D. Water Dynamics in Large and Small Reverse Micelles: From Two Ensembles to Collective Behavior. *J. Chem. Phys.* **2009**, *131*, 014704.
(40) Moilanen, D. E.; Piletic, I. R.; Fayer, M. D. Water Dynamics in Nafion Fuel Cell Membranes: The Effects of Confinement and Structural Changes on the Hydrogen Bond Network. *J. Phys. Chem. C* **2007**, *111*, 8884−8891.
(41) Le Caër, S.; Lima, M.; Gosset, D.; Simeone, D.; Bergaya, F.; Pommeret, S.; Renault, J.-P.; Righini, R. Dynamics of Water Confined in Clay Minerals. *J. Phys. Chem. C* **2012**, *116*, 12916−12925.
(42) Hung, S. T.; Yamada, S. A.; Zheng, W.; Fayer, M. D. Ultrafast Dynamics and Liquid Structure in Mesoporous Silica: Propagation of Surface Effects in a Polar Aprotic Solvent. *J. Phys. Chem. B* **2021**, *125*, 10018−10034.
(43) Gera, R.; Meloni, S. L.; Anna, J. M. Unraveling Confined Dynamics of Guests Trapped in Self-Assembled Pd_6L_4 Nanocages by Ultrafast Mid-IR Polarization-Dependent Spectroscopy. *J. Phys. Chem. Lett.* **2019**, *10*, 413−418.
(44) Kenkre, V.; Tokmakoff, A.; Fayer, M. Theory of Vibrational Relaxation of Polyatomic Molecules in Liquids. *J. Chem. Phys.* **1994**, *101*, 10618−10629.
(45) Widegren, J. A.; Laesecke, A.; Magee, J. W. The Effect of Dissolved Water on the Viscosities of Hydrophobic Room-Temperature Ionic Liquids. *Chem. Commun.* **2005**, 1610−1612.
(46) Tamimi, A.; Fayer, M. D. Ionic Liquid Dynamics Measured with 2D IR and IR Pump-Probe Experiments on a Linear Anion and

https://doi.org/10.1021/acs.jpcb.3c02948
J. Phys. Chem. B XXXX, XXX, XXX−XXX

the Influence of Potassium Cations. *J. Phys. Chem. B* **2016**, *120*, 5842−5854.
(47) Levin, D. E.; Schmitz, A. J.; Hines, S. M.; Hines, K. J.; Tucker, M. J.; Brewer, S. H.; Fenlon, E. E. Synthesis and Evaluation of the Sensitivity and Vibrational Lifetimes of Thiocyanate and Selenocyanate Infrared Reporters. *RSC Adv.* **2016**, *6*, 36231−36237.
(48) Maj, M.; Kwak, K.; Cho, M. Ultrafast Structural Fluctuations of Myoglobin-Bound Thiocyanate and Selenocyanate Ions Measured with Two-Dimensional Infrared Photon Echo Spectroscopy. *ChemPhysChem* **2015**, *16*, 3468−3476.
(49) Ohta, K.; Tominaga, K. Vibrational Population Relaxation of Thiocyanate Ion in Polar Solvents Studied by Ultrafast Infrared Spectroscopy. *Chem. Phys. Lett.* **2006**, *429*, 136−140.
(50) Shim, S.-H.; Strasfeld, D. B.; Fulmer, E. C.; Zanni, M. T. Femtosecond Pulse Shaping Directly in the Mid-IR Using Acousto-Optic Modulation. *Opt. Lett.* **2006**, *31*, 838−840.
(51) Shim, S.-H.; Zanni, M. T. How to Turn Your Pump-Probe Instrument into a Multidimensional Spectrometer: 2D IR and Vis Spectroscopies Via Pulse Shaping. *Phys. Chem. Chem. Phys.* **2009**, *11*, 748−761.
(52) Tokmakoff, A. Orientational correlation functions and polarization selectivity for nonlinear spectroscopy of isotropic media. I. Third order. *J. Chem. Phys.* **1996**, *105*, 1−12.
(53) Tan, H.-S.; Piletic, I. R.; Fayer, M. Polarization Selective Spectroscopy Experiments: Methodology and Pitfalls. *J. Opt. Soc. Am. B* **2005**, *22*, 2009−2017.
(54) Kore, S.; Sahoo, R. R.; Santra, B.; Sarkar, A.; Chowdhury, T.; Deshmukh, S. H.; Hazarika, S.; Chatterjee, S.; Bagchi, S. Solvation Structure and Dynamics of a Small Ion in an Organic Electrolyte. *J. Photochem. Photobiol., A* **2023**, *440*, 114666.
(55) Okuda, M.; Ohta, K.; Tominaga, K. Comparison of Vibrational Dynamics between Non-Ionic and Ionic Vibrational Probes in Water: Experimental Study with Two-Dimensional Infrared and Infrared Pump-Probe Spectroscopies. *J. Chem. Phys.* **2016**, *145*, 114503.
(56) Schultz, P. Ab Initio Calculations of Ionic and Hydrogen Bonding Interactions with the OCN^-, SCN^- and $SeCN^-$ Anions. *Mol. Phys.* **1996**, *88*, 217−246.
(57) Biswas, A.; Mallik, B. S. Molecular Simulation-Guided Spectroscopy of Imidazolium-Based Ionic Liquids and Effects of Methylation on Ion-Cage and-Pair Dynamics. *J. Phys. Chem. B* **2022**, *126*, 8838−8850.
(58) Wang, Y.-L.; Li, B.; Sarman, S.; Mocci, F.; Lu, Z.-Y.; Yuan, J.; Laaksonen, A.; Fayer, M. D. Microstructural and Dynamical Heterogeneities in Ionic Liquids. *Chem. Rev.* **2020**, *120*, 5798−5877.
(59) Dong, K.; Zhang, S.; Wang, D.; Yao, X. Hydrogen Bonds in Imidazolium Ionic Liquids. *J. Phys. Chem. A* **2006**, *110*, 9775−9782.
(60) Lungwitz, R.; Friedrich, M.; Linert, W.; Spange, S. New Aspects on the Hydrogen Bond Donor (HBD) Strength of 1-Butyl-3-Methylimidazolium Room Temperature Ionic Liquids. *New J. Chem.* **2008**, *32*, 1493−1499.
(61) Gunda, N. S. K.; Singh, M.; Norman, L.; Kaur, K.; Mitra, S. K. Optimization and Characterization of Biomolecule Immobilization on Silicon Substrates Using (3-Aminopropyl) Triethoxysilane (APTES) and Glutaraldehyde Linker. *Appl. Surf. Sci.* **2014**, *305*, 522−530.
(62) Montalbán, M.; Bolívar, C.; Diaz Banos, F. G.; Víllora, G. Effect of Temperature, Anion, and Alkyl Chain Length on the Density and Refractive Index of 1-Alkyl-3-Methylimidazolium-Based Ionic Liquids. *J. Chem. Eng. Data* **2015**, *60*, 1986−1996.
(63) Ue, M. Mobility and Ionic Association of Lithium and Quaternary Ammonium Salts in Propylene Carbonate and γ-Butyrolactone. *J. Electrochem. Soc.* **1994**, *141*, 3336.
(64) Yamada, S. A.; Thompson, W. H.; Fayer, M. D. Water-Anion Hydrogen Bonding Dynamics: Ultrafast IR Experiments and Simulations. *J. Chem. Phys.* **2017**, *146*, 234501.
(65) Kramer, P. L.; Giammanco, C. H.; Fayer, M. D. Dynamics of Water, Methanol, and Ethanol in a Room Temperature Ionic Liquid. *J. Chem. Phys.* **2015**, *142*, 212408.
(66) Yamada, S. A.; Hung, S. T.; Thompson, W. H.; Fayer, M. D. Effects of Pore Size on Water Dynamics in Mesoporous Silica. *J. Chem. Phys.* **2020**, *152*, 154704.
(67) Chen, S.; Voth, G. A. How Does Electronic Polarizability or Scaled-Charge Affect the Interfacial Properties of Room Temperature Ionic Liquids? *J. Phys. Chem. B* **2023**, *127*, 1264−1275.
(68) Amith, W. D.; Hettige, J. J.; Castner Jr, E. W.; Margulis, C. J. Structures of Ionic Liquids Having Both Anionic and Cationic Octyl Tails: Lamellar Vacuum Interface Vs Sponge-Like Bulk Order. *J. Phys. Chem. Lett.* **2016**, *7*, 3785−3790.
(69) Coasne, B.; Fourkas, J. T. Structure and Dynamics of Benzene Confined in Silica Nanopores. *J. Phys. Chem. C* **2011**, *115*, 15471−15479.
(70) Zhu, X.; Farrer, R. A.; Fourkas, J. T. Ultrafast Orientational Dynamics of Nanoconfined Benzene. *J. Phys. Chem. B* **2005**, *109*, 12724−12730.
(71) Loughnane, B. J.; Farrer, R. A.; Scodinu, A.; Fourkas, J. T. Dynamics of a Wetting Liquid in Nanopores: An Optical Kerr Effect Study of the Dynamics of Acetonitrile Confined in Sol-Gel Glasses. *J. Chem. Phys.* **1999**, *111*, 5116−5123.

https://doi.org/10.1021/acs.jpcb.3c02948
J. Phys. Chem. B XXXX, XXX, XXX−XXX